Design and Finite Element Analysis of E-glass Fiber Reinforced Epoxy Composite Air Bottle used in Missile System: Experimental Validation

A. Chennakesava Reddy

Abstract— The objective of this paper was to design the air bottle used in military system and to validate the design using finite element analysis. The load bearing capacity of the air bottle was 40 MPa. The air bottle was made of E-glass/epoxy composite. The hoop and helical winding layer thicknesses were, respectively, 3.6 3.013 mm. Matrix splitting was occurred along the fibers. The fibers were broken when the air bottle was tested at a pressure of 60 MPa.

Index Terms— E-glass/epoxy composite, air bottle, hoop winding, helical winding,

1 INTRODUCTION

PRESSURE vessels are being used for storage of high pressure gases for industrial purpose and aerospace applications. In missiles, pressure vessel or air bottles are used as power source to actuate various mechanisms for control and stability of the vehicle. As weight is main concern in aerospace vehicles, weight is optimized at each and every step. The air bottles used in missiles are pressurized at high pressure (nearly 400 bars) which itself is a live bomb to explode in minor defects. To reduce its weight and to avoid catastrophic failures, these days pressure vessels are designed with fiber reinforced plastic (FRP) composites.

Steven Cambell [1] has described an innovative method of CNG transportation. The method utilizes composite pressure vessels which are derived from the national defense / aerospace, and natural gas vehicle industries. The method overcomes all of the deficiencies anticipated from other proposed methods of CNG transportation that propose to use steel based gas containment systems. The proposed CPV (composite pressure vessel) designed for the Trans Ocean Gas CNG transportation method is between 42 and 44 inches in diameter by approximately 40 feet long. The pressure rating of the proposed CPV is up to 3600 psi. CPVs are manufactured by winding a filament fiber over an HDPE liner. The liner with hemispherical end caps forms a mandrel, which is installed on a computer controlled automatic winder. The ends of the liner are equipped with a stainless steel port boss for future welding of the CPV to conventional piping. As the filament is wound over the mandrel, it is drawn through an epoxy bath at constant tension. The end result is a helically wound fiber formation set in an epoxy matrix. The two most common filament fibers used to manufacture CPVs are carbon and glass. A patent US5287987A by Gaiser William [2] describes a light weight filament wound pressure vessel for retaining gases under high pressure, formed with a barrier liner, in which the liner comprises a single layer of biaxially stretched and oriented polyethylene terephthalate (PET) plastic material.

Glass fibers currently comprise more than 90% of the fibers used in polymer composites. There are five major types of glass used to make glass fibers. These are A-glass (high alkali), C-glass (chemical), D-glass (low dielectric constant), E-glass (electrical) and S-glass (high strength), out of which the last two types, due to their superior mechanical properties, are most widely used in composite roofings, pressure vessels, containers, tanks, pipes, etc. E- glass is a low alkali, aluminum boro solicate glass and is based on a mixture of alumina, boric acid, calcium carbonate and magnesia [3]. Epoxies are thermosetting polymer resins where the resin molecule contains one or more epoxide groups. Epoxy resins are cured with the addition of a curing agent, which is commonly called a hardener. Perhaps the most common type of curing agent is amine based. Attributes of epoxy resins include extremely low shrinkage, good dimensional stability, high temperature resistance, good fatigue and adherence to reinforcements [4-7].

This paper dealt with design and finite element analysis of fiber reinforced plastic composite air bottle. Here, a pressure vessel made up of steel used in a missile system, was designed using composites of glass fiber/epoxy. This pressure vessel was used as a power source to actuate the different mechanisms during the flight.

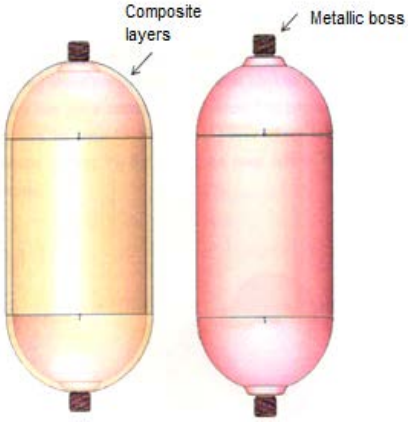

Fig. 1. The composite pressure vessel.

• *A. Chennakesava Reddy is Professor and BOS Chairman of Mechanical Engineering, JNT University, Hyderabad, India, Mobile-9440568776. E-mail: acreddy@jntuh.ac.in*

ISSN 2229-5518

2 MATERIALS AND METHODS

The pressure vessel consists of a metallic inner liner, a metallic boss and composite layers over the liner as shown in figure 1. The inner metallic liner was required for leak proofing of the vessel. Being a cylindrical shell with hemispherical end domes along with symmetrical opening along the axis, filament winding method was used for laying the composite layers over the metallic liner.

2.1 Design of Composite Pressure Vessel

Metallic liner is used as a leak proof layer. It was made of 1mm thickness of titanium (Ti-6Al-4V) sheet. Metallic boss is an integral component of FRP pressure vessel. It was made of metallic material (steel) because of its complicated shape and complex mode of loading where the composite materials could not be reliable. Metallic boss has got a passage which is used to pressurize the cylinder with air and to release the same for utilization as power source to drive the different mechanisms in missile system. Figure 2 shows the boss used in pressure vessel.

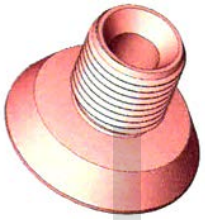

Fig. 2. The metallic boss.

Major failures in the boss could be: (1) it can be thrown out of the pressure vessel at its limiting loading condition and (2) shearing of threads. The first mode of failure ca ne avoided with sufficient number of layers of FRp on the steel boss during the filament winding. The second mode of failure can be avoided by proper selection of diameter type of thread, length of engagement and material used.

Force acting on threads = P X A (1)

$$= 40 \times \pi \times 18^2/4 = 10173.6\,N$$

where, P is the internal pressure in cylinder and A is the projected area.

Average screw thread shearing stress is obtained by assuming that the load is uniformly distributed over the nut height, h, and threads shears off at minor diameter of the threaded portion in the boss.

Shear stress, $\tau = 2F/\pi d_r h$ (2)

where, F is the force on threads, d_r is the minor diameter and h is the height of the engagement of nut.

Threads on nut shear off at the major diameter. Shearing stress on the nut is given as follows:

Shear stress, $\tau = 2F/\pi dh$ (3)

where d is the major diameter.

Alloy 15CDV6 is a low carbon steel which combines high yield strength (superior to SAE 4130) with good toughness and weldability. 15CDV6 can be readily welded with very little loss of properties during welding and without the need for further heat treatment. This alloy finds many applications in the aerospace and motorsports industries in such components as roll cages, pressure vessels, suspensions, rocket motor casings, wish bones and subframes. For 15 CDV6, shearing stress is 600 MPa. For a factor of safety of 1.5, the allowable shear strength = 333 MPa.

Taking the thread standard of M18x1.5, the shearing stress in the threads of boss from Eq. (2) is obtained as follows:

Shear stress, $\tau = (2x10173.6)/(\pi*16.16x1.5) = 26.73$ *MPa.*

Since 26.73 < 333 MPa, hence, the design is safe.

Shearing stress on the nut is obtained from Eq. (3) as follows:

Shear stress, $\tau = (2x10173.6)/(\pi*18x1.5) = 24$ *MPa.*

Since 24 < 333 MPa, hence, the design is safe.

If the filament-wound pressure vessel has a diameter of D and an internal pressure of P, its overall thickness is composed of longitudinal windings of thickness t_l, hoop windings of thickness t_h and helical windings of thickness t_θ which are applied at an angle θ to the longitudinal axis of the cylindrical vessel. Let us also assume that each filament in any of the windings is stressed by the same amount, σ_w. for any cylindrical pressure vessel with end plates, the loading or stress in the wall of the vessel can be resolved into two components, the longitudinal component, σ_l acting parallel to the axis of the cylinder and the hoop stress, σ_h. Since the pressure vessel is symmetrical, the shear stress is zero along the principle axes. The hoop stress depends on the internal pressure, vessel diameter and vessel wall thickness. The hoop stress is calculated using the formula given below:

$$\sigma_h = PD/2t \quad (4)$$

The hoop stress is always twice that of the longitudinal stress. The longitudinal stress is given below:

$$\sigma_l = \sigma_h/2 \quad (5)$$

Since the shell of the vessel under consideration is made of hoop, longitudinal and helical windings, the hoop stress will be the sum of the components of stress in the hoop windings, the hoop stress component produced by the helical winding, the longitudinal winding. The longitudinal components of the helical windings act at right angles and do not contribute to the hoop stress. By a force balance per unit length of wall cross-section parallel to the axis of cylinder:

$$\sigma_h = \acute{\sigma_h}\, t_h/t + \sigma_{h\theta}\, t_\theta/t \quad (6)$$

where, $\acute{\sigma_h}$ is the stress in the hoop winding layer and $\sigma_{h\theta}$ is the hoop component of stress in the wall contributed by the helical winding.

Similarly the longitudinal stress is given as follows:

$$\sigma_l = \acute{\sigma_l}\, t_l/t + \sigma_{l\theta}\, t_\theta/t \quad (7)$$

where, $\acute{\sigma_l}$ is the stress in the longitudinal winding layer and $\sigma_{l\theta}$ is the longitudinal component of stress in the wall contributed by the helical winding.

From Eq. (5), we get the following relation:

$$\sigma_h/2 = \acute{\sigma_l}\, t_l/t + \sigma_{l\theta}\, t_\theta/t \quad (8)$$

According assumption that that each filament in any of the windings is stressed by the same amount, σ_w, we get the

following relation:

$$\sigma_h = \sigma_l = \sigma_w \quad (9)$$

We can develop the following relationship based on the geometry of two of the filaments of the helical windings (figure 3):

$$2\sigma_w A\sin\theta = \sigma_{h\theta}\, 2A/\sin\theta \quad (10)$$

$$\sigma_{h\theta} = \sigma_w \sin^2\theta \quad (11)$$

And similarly the longitudinal component of the helical winding stress:

$$\sigma_{l\theta} = \sigma_w \cos^2\theta \quad (12)$$

If Eqs. (11) and (12) are added, we get the following relation:

$$\sigma_{h\theta} + \sigma_{l\theta} = \sigma_w \sin^2\theta + \sigma_w \cos^2\theta = \sigma_w \quad (13)$$

Therefore, at all times the stresses in all winding filaments are equal.

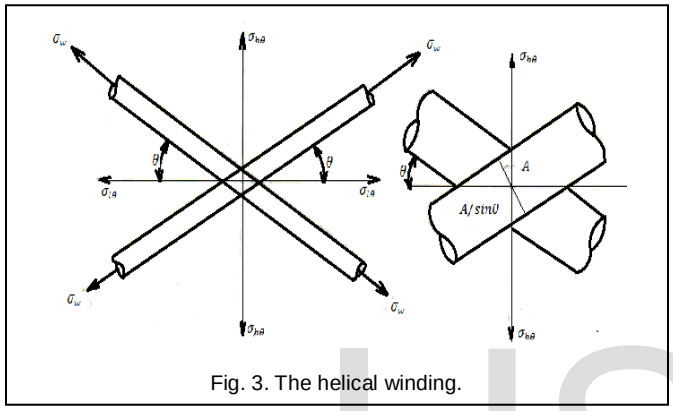

Fig. 3. The helical winding.

The total thickness of winding is given below:

$$t = t_l + t_h + t_\theta \quad (14)$$

By substitution Eq. (6) and Eq. (9) becomes:

$$\sigma_h = \sigma_{th}/t + \sigma_w t_\theta \sin^2\theta/t \quad (15)$$

By substitution Eq. (7) and Eq. (9) becomes:

$$\sigma_l = \sigma_{tl}/t + \sigma_w t_\theta \cos^2\theta/t \quad (16)$$

By adding Eq. (15) and Eq. (16), we get the following relation:

$$\sigma_w = \sigma_h + \sigma_l \quad (17)$$

With this relationship it is possible to develop the formula for the overall thickness of filament wound vessel.

We know that , $\sigma_h = 2\sigma_l = PD/2t$ (18)

By rearranging Eq. (18), we get

$$t = PD/4\sigma_l \quad (19)$$

And by Eq. (17) and Eq.(18), we get the following relation:

$$\sigma_l = \sigma_w/3 \quad (20)$$

Hence, Eq.(19) becomes:

$$t = 3PD/4\sigma_w \quad (21)$$

If P, D and σw are known it is possible to determine the overall thickness of the filament wound vessel. The overall wall thickness does not depend on the thickness of the individual winding layers or on the helical winding angle. It is dependent only on the diameter of the vessel, the internal pressure and the allowable fiber stress.

Remembering that the hoop stress is twice the longitudinal stress and using Eqs. (15) and (16), we obtain:

$$\sigma_{th} + \sigma_w t_\theta \sin^2\theta/t = 2\sigma_{tl} + 2\sigma_w t_\theta \cos^2\theta \quad (22)$$

$$t_\theta = 2t_l - t_h/(\sin^2\theta - 2\cos^2\theta) \quad (23)$$

$$t_\theta = (2t_l - t_h)/(1 - 3\cos^2\theta) \quad (24)$$

Since, $\sin^2\theta = 1 - \cos^2\theta$.

By solving Eqs. (12) and (22) simultaneously (subtracting Eq. (24) from Eq. (14) to solve for t_l and then using Eq. (12) to solve for t_h, the following expressions result:

$$t_l = t/3 - t_\theta \cos^2\theta \quad (25)$$

$$t_h = 2t/3 - t_\theta \sin^2\theta \quad (26)$$

Finally,

The overall wall thickness, $t = 3PD/4\sigma_w$

Hoop winding thickness, $t_h = 2t/3 - (t - t_h)\sin^2\theta$

Helical winding thickness, $t_\theta = (2t - 3t_h)/3\sin^2\theta$

For E-glass/epoxy UD lamina:
Ultimate tensile strength = 1062 = MPa
Factor of safety = 2
Allowable tensile strength, σ_w = 531 MPa
Shell diameter, D = 115.5 m
Internal pressure, P = 40 MPa
Helical angle, θ = 30°

The following thicknesses are calculated:
The overall thickness, t = 3PD/4 σ_w = 6.53 mm.
Hoop winding thickness = 3.6 mm
Helical winding thickness = 3.013 mm

Hence, a hoop layer of 3.6 mm thickness over the metallic liner and helical winding layer of 3.013 mm thickness over the hoop layer will be sufficient to take the load of 40 MPa. For the verification these results, lay-up thickness are modeled using finite element analysis.

2.2 Finite Element Analysis

The design verification glass fiber/epoxy composite pressure vessel was carried out using Finite element analysis software PATAN and analyzed using MSC-NASTRAN. The finite element modeling was done considering the symmetry of the air bottle in terms of the loads, boundary conditions, geometry and material properties. Therefore, only the half portion of the air bottle was modeled with appropriate boundary condition.

The input specifications are as follows:
Mean diameter of the bottle = 115.5 mm
Internal pressure = 40 MPa
Thickness of the bottle = 6.5 mm
Hoop winding thickness = 3.6 mm
Helical winding thickness = 3.013 mm

The geometry of the air bottle is shown in figure 4. It has one cylindrical portion of mean diameter of 115 mm and length of 140 mm bounded by two hemispherical end domes. The total length of the air bottle is 261 mm. The material properties were calculated at room temperature and the strength properties were taken at room temperature. The properties of E-glass/epoxy unidirectional (UD) are given in table 1. The density of E-glass/epoxy is, ρ = 1.86 g/cc. The strength properties are given in table 2.

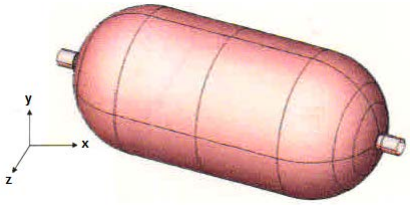

Fig. 4. Geometric modeling of air bottle.

TABLE 1

PROPERTIES OF E-GLASS/EPOXY (UD)

Elastic modulus,	Poisson's ratio	Shear modulus
E_x = 34.4 GPa	ν_x =0.27	G_x = 2.94 GPa
E_y = 9.67 GPa	ν_y =0.27	G_y = 2.94 GPa
E_z = 9.67 GPa	ν_z =0.27	G_z =3.4 GPa

TABLE 2

STRENGTH PROPERTIES OF E-GLASS/EPOXY (UD) AND STEEL

Property	Value
E-glass/epoxy (UD)	
Longitudinal tensile strength	1062 MPa
Longitudinal compressive strength	610 MPa
Transverse tensile strength	31 MPa
Transverse compressive strength	110 MPa
In-plane shear strength	72 MPa
Steel	
Elastic modulus	207 GPa
Poisson's ratio	0.3
Density	7.88 g/cc

Fig. 5. Four-axis CNC machine filament winding of air bottle.

For pressure vessels such as LPG or CNG containers (for example) it is normal to have a four-axis winding machine (figure 5). A four-axis machine additionally has a radial (cross-feed) axis perpendicular to carriage travel and a rotating fiber payout head mounted to the cross-feed axis. The payout head rotation can be used to stop the fiber band twisting and thus varying in width during winding. The lay-up details of the cylindrical section are given table 3. The lay-up at joint of composite layer and boss was divided into four segments. In this portion the combination of composite and steel was used. The lay-up details for the four segments are given table 4 to 7. The lay-up details are given in table 8.

The GFRP composite pressure bottle is the space product fabricated by continuous winding of E-glass fibers in an epoxy resin matrix over the polypropylene liner. The winding was done using two basic wraps. The first basic wrap, called helical winding, was laid at a fixed angle of 30° from the longitudinal axis of the bottle. The second basic wrap, called hoop winding, was laid at an angle of 90° to the longitudinal axis. The total 6.5mm wall thickness of the FRP shell is contributed by 16 helical layers and 18 hoop layers.

TABLE 3

LAY-UP DETAILS FOR THE CYLINDRICAL SECTION

Material	Thickness	Orientation	Global ply id
Glass/epoxy	0.2	90	1 to 18
Glass/epoxy	0.2	30	19
Glass/epoxy	0.2	-30	20
Glass/epoxy	0.2	30	21
Glass/epoxy	0.2	-30	22
Glass/epoxy	0.2	30	23
Glass/epoxy	0.2	-30	23
Glass/epoxy	0.2	30	25
Glass/epoxy	0.2	-30	26
Glass/epoxy	0.2	30	27
Glass/epoxy	0.2	-30	28
Glass/epoxy	0.2	30	29
Glass/epoxy	0.2	-30	30
Glass/epoxy	0.2	30	31
Glass/epoxy	0.2	-30	32
Glass/epoxy	0.2	30	33
Glass/epoxy	0.2	-30	34

TABLE 4

LAY-UP DETAILS FOR THE FIRST SEGMENT OF STEEL AND COMPOSITE COMBINATION

Material	Thickness	Orientation	Global ply id
steel	1.3	0	100
Glass/epoxy	0.2	90	9 to 18
Glass/epoxy	0.2	30	19
Glass/epoxy	0.2	-30	20
Glass/epoxy	0.2	30	21
Glass/epoxy	0.2	-30	22
Glass/epoxy	0.2	30	23
Glass/epoxy	0.2	-30	23
Glass/epoxy	0.2	30	25
Glass/epoxy	0.2	-30	26
Glass/epoxy	0.2	30	27
Glass/epoxy	0.2	-30	28
Glass/epoxy	0.2	30	29
Glass/epoxy	0.2	-30	30
Glass/epoxy	0.2	30	31
Glass/epoxy	0.2	-30	32
Glass/epoxy	0.2	30	33
Glass/epoxy	0.2	-30	34

TABLE 5

LAY-UP DETAILS FOR THE SECOND SEGMENT OF STEEL AND COMPOSITE COMBINATION

Material	Thickness	Orientation	Global ply id
steel	1.3	0	100
steel	1.3	0	101
Glass/epoxy	0.2	90	15 to 18
Glass/epoxy	0.2	30	19
Glass/epoxy	0.2	-30	20
Glass/epoxy	0.2	30	21
Glass/epoxy	0.2	-30	22
Glass/epoxy	0.2	30	23
Glass/epoxy	0.2	-30	23
Glass/epoxy	0.2	30	25
Glass/epoxy	0.2	-30	26
Glass/epoxy	0.2	30	27
Glass/epoxy	0.2	-30	28
Glass/epoxy	0.2	30	29
Glass/epoxy	0.2	-30	30
Glass/epoxy	0.2	30	31
Glass/epoxy	0.2	-30	32
Glass/epoxy	0.2	30	33
Glass/epoxy	0.2	-30	34

TABLE 6

LAY-UP DETAILS FOR THE THIRD SEGMENT OF STEEL AND COMPOSITE COMBINATION

Material	Thickness	Orientation	Global ply id
steel	1.3	0	100
steel	1.3	0	101
steel	1.3	0	102
Glass/epoxy	0.2	-30	20
Glass/epoxy	0.2	30	21
Glass/epoxy	0.2	-30	22
Glass/epoxy	0.2	30	23
Glass/epoxy	0.2	-30	23
Glass/epoxy	0.2	30	25
Glass/epoxy	0.2	-30	26
Glass/epoxy	0.2	30	27
Glass/epoxy	0.2	-30	28
Glass/epoxy	0.2	30	29
Glass/epoxy	0.2	-30	30
Glass/epoxy	0.2	30	31
Glass/epoxy	0.2	-30	32
Glass/epoxy	0.2	30	33
Glass/epoxy	0.2	-30	34

The loads and boundary conditions are as follows:
The Discretization of the air bottle is shown in figure 6. The internal pressure of 40 MPa was applied to the air bottle. To simulate the complete air bottle, only half portion was modeled and symmetric boundary condition was given at the nodes mid section. The boundary conditions were applied in cylindrical coordinates at the nodes to simulate the actual conditions. The loads and boundary conditions are shown in figure 7.

TABLE 7

LAY-UP DETAILS FOR THE FOURTH SEGMENT OF STEEL AND COMPOSITE COMBINATION

Material	Thickness	Orientation	Global ply id
steel	1.3	0	100
steel	1.3	0	101
steel	1.3	0	102
steel	1.3	0	103
Glass/epoxy	0.2	30	29
Glass/epoxy	0.2	-30	30
Glass/epoxy	0.2	30	31
Glass/epoxy	0.2	-30	32
Glass/epoxy	0.2	30	33
Glass/epoxy	0.2	-30	34

TABLE 8

LAY-UP DETAILS FOR THE HEMISPHERICAL DOME

Material	Thickness	Orientation	Global ply id
Glass/epoxy	0.2	90	1 to 18
Glass/epoxy	0.2	30	19
Glass/epoxy	0.2	-30	20
Glass/epoxy	0.2	30	21
Glass/epoxy	0.2	-30	22
Glass/epoxy	0.2	30	23
Glass/epoxy	0.2	-30	23
Glass/epoxy	0.2	30	25
Glass/epoxy	0.2	-30	26
Glass/epoxy	0.2	30	27
Glass/epoxy	0.2	-30	28
Glass/epoxy	0.2	30	29
Glass/epoxy	0.2	-30	30
Glass/epoxy	0.2	30	31
Glass/epoxy	0.2	-30	32
Glass/epoxy	0.2	30	33
Glass/epoxy	0.2	-30	34

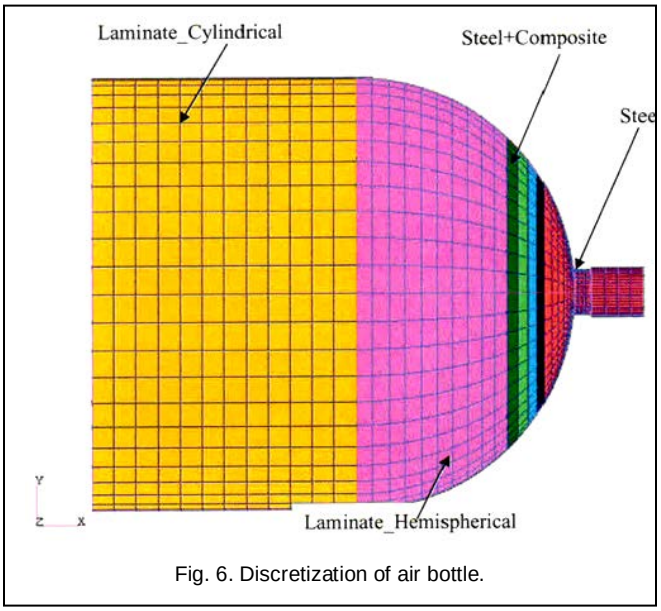

Fig. 6. Discretization of air bottle.

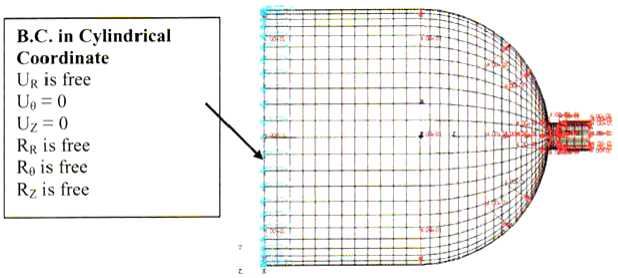

Fig. 7. Loads and boundary conditions.

2.3 Testing Procedure of GFRP Pressure Bottles

The entire surface of the GFRP pressure bottle was thoroughly cleaned with liquid acetone. Strain gauges of 350 ohm, (0-18000 με) were bonded at six different locations on the bottle, such as two on the (helical winding) end domes and four on the (hoop winding) cylindrical portion. All of them were connected to a 30 channel data acquisition system (DAQ) to enable online monitoring and recording of the data during testing. The bottle was filled with water and the open end was connected to the outlet of the Haskel air operated water pump. Four R-15 AE sensors (150 kHz, resonant) were mounted over the bottle, two at the end domes (fill end, closed end) 180° to each other, and the other two at the middle of the cylindrical portion 180° apart. The locations of these two sensors make a 90° angle with the earlier two, so that the entire volume of the bottle was within the vicinity of the sensors. All the sensors were connected with the AE workstation through 1220 amp. preamplifiers by means of shielded connecting cables. The axial and diametrical dilations of the bottle were measured by three linear potentiometers (0-10mm range); two were mounted at the end adapters (fill end, closed end) and one at the top middle portion of cylindrical region of the vessel as shown in figure 8.

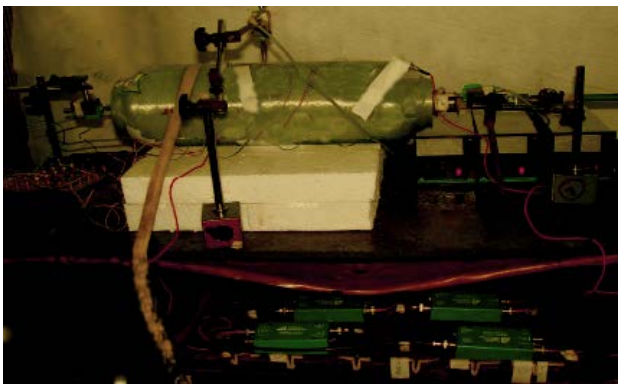

Fig. 8. Hydrostatic test setup on the composite air bottle.

3 Results and Discussion

The deformation plot is shown in figure 8. The maximum displacement was found to be 0.0467 microns. The stress induced in the boss is shown in figure 10. The maximum stress was 0.477 MPa.

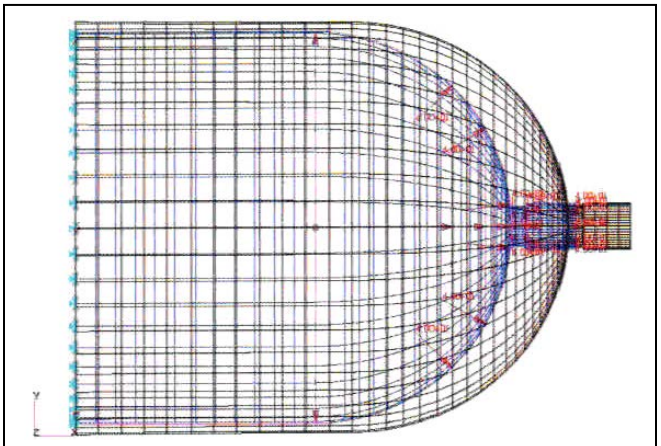

Fig. 9. Deformation of composite air bottle.

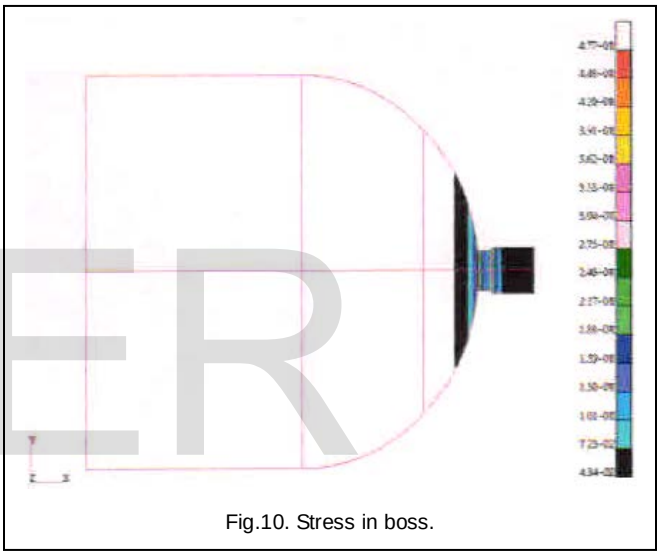

Fig.10. Stress in boss.

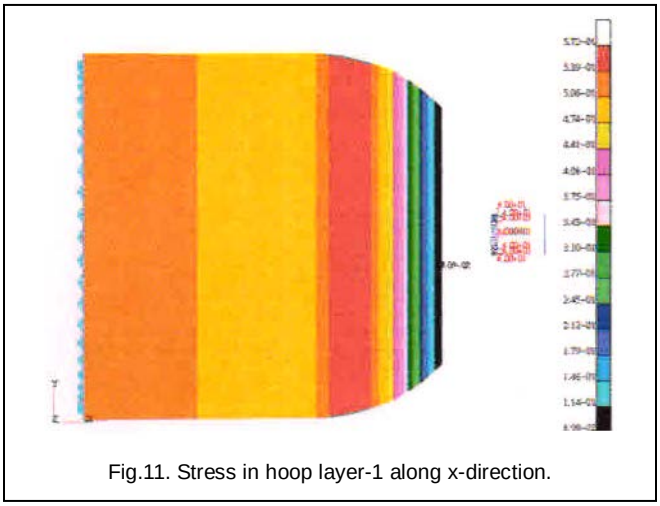

Fig.11. Stress in hoop layer-1 along x-direction.

The stresses in the hoop layer-1 along x-, y- and z- directions are depicted in figures 11, 12 and 13 respectively. The maximum stresses were 0.573, 0.109 and 0.0000149 MPa along x-, y- and z- directions respectively. The stresses in the hoop layer-18 along x-, y- and z- directions are depicted in figures 14, 15

and 16 respectively. The maximum stresses were 0.518, 0.0406 and 0.00000272 MPa along x-, y- and z- directions respectively.

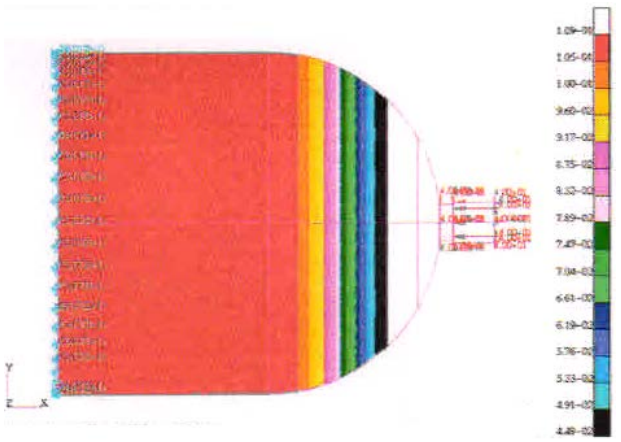

Fig.12. Stress in hoop layer-1 along y-direction.

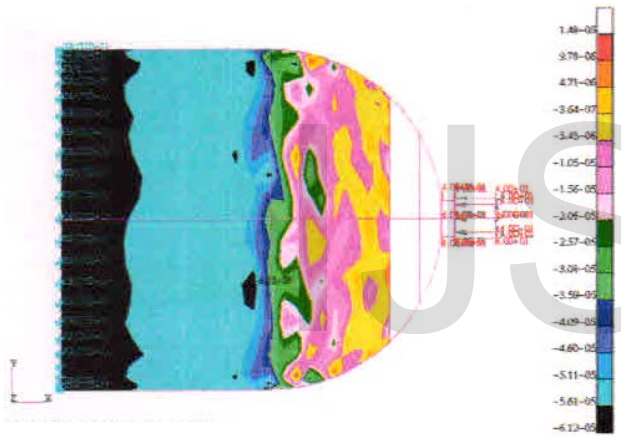

Fig.13. Stress in hoop layer-1 along z-direction.

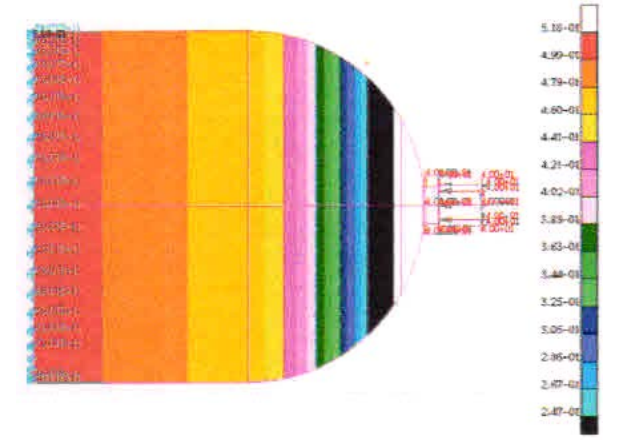

Fig.14. Stress in hoop layer-18 along x- direction

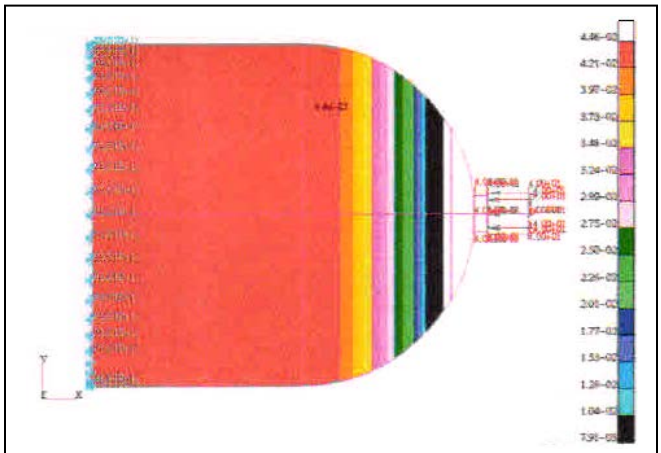

Fig.15. Stress in hoop layer-18 along y- direction.

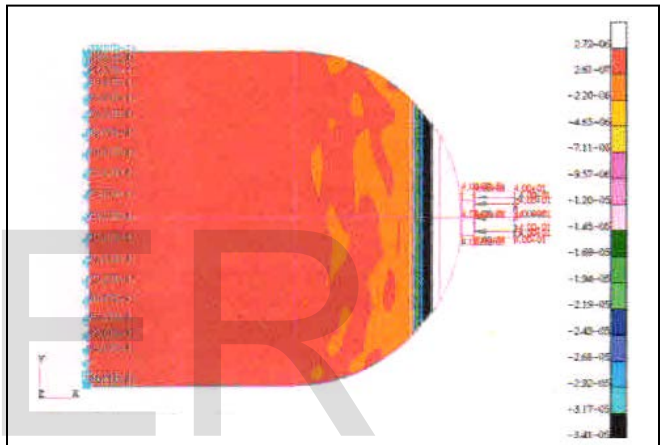

Fig.16. Stress in hoop layer-18 along z-direction.

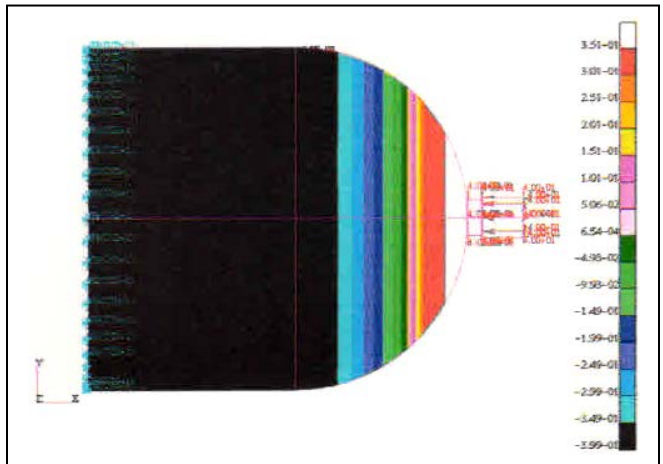

Fig.17. Stress in helical layer-34 along x-direction.

The stresses in the helical layer-34 along x-, y- and z- directions are depicted in figures 17, 18 and 19 respectively. The maximum stresses were 0.351, 0.00152 and -0.000715 MPa along x-, y- and z- directions respectively.

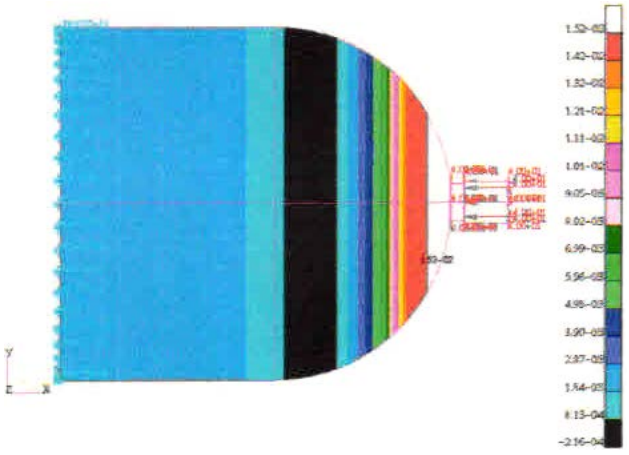

Fig.18. Stress in helical layer-34 along y- direction.

Fig.19. Stress in helical layer-34 along L-T direction.

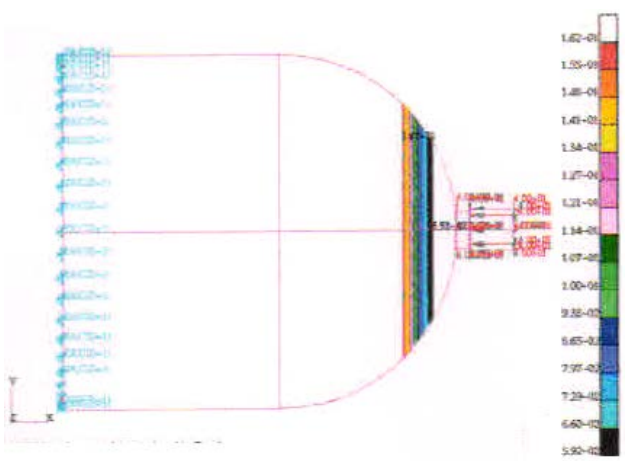

Fig.20. Stress in steel layer 100.

The stresses in the steel layers -100, 101, 102 and 103 are illustrated in figures 20, 21, 22 and 23 respectively. The maximum stresses were 0.162, 0.189, 0.186 and 0.254 MPa respectively.

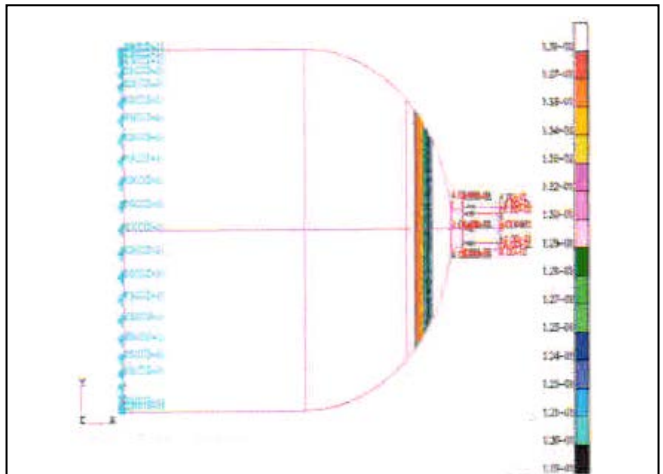

Fig.21. Stress in steel layer 101.

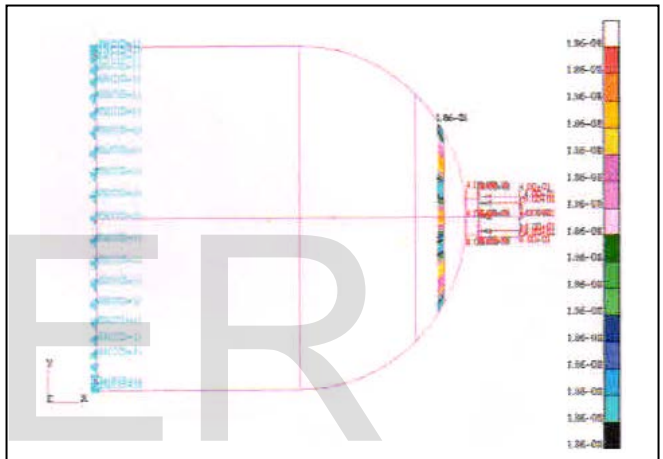

Fig.22. Stress in steel layer 102.

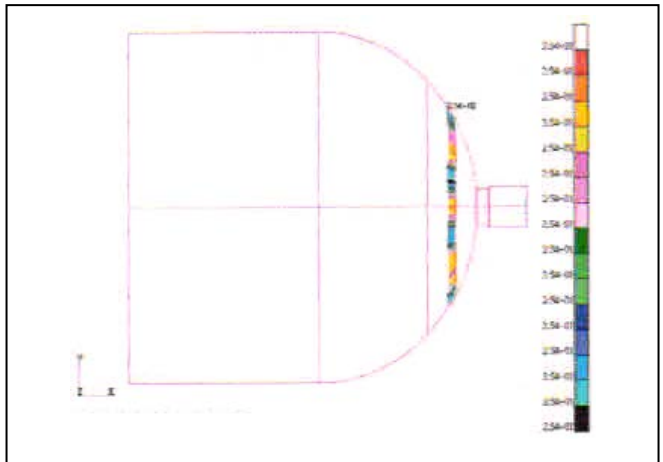

Fig.23. Stress in steel layer 103.

4 Experimental Validation

A hydrostatic pressure test was carried out on the bottle up to its theoretical burst pressure of 40 MPa bar in a cyclic mode and the acoustic emission (AE), strain, and dilation data were acquired.

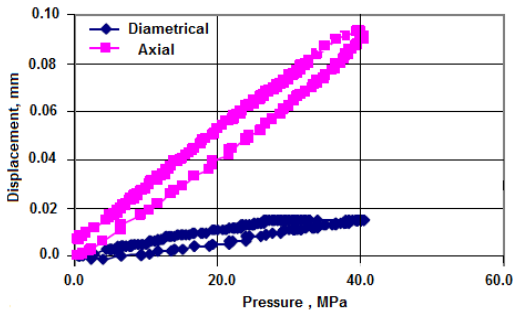

Fig.24. Displacement of air bottle under pressure loading.

Fig.25. Tensile test specimen.

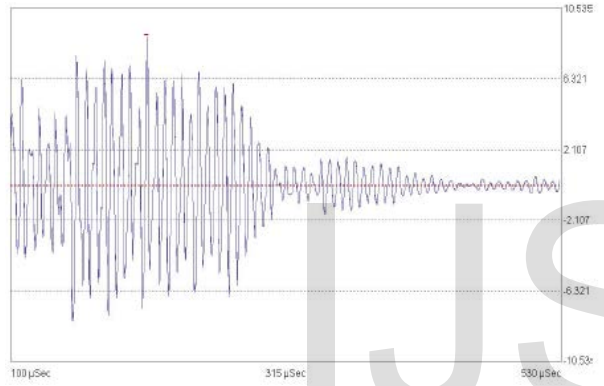

Fig.26. Wave form of matrix splitting.

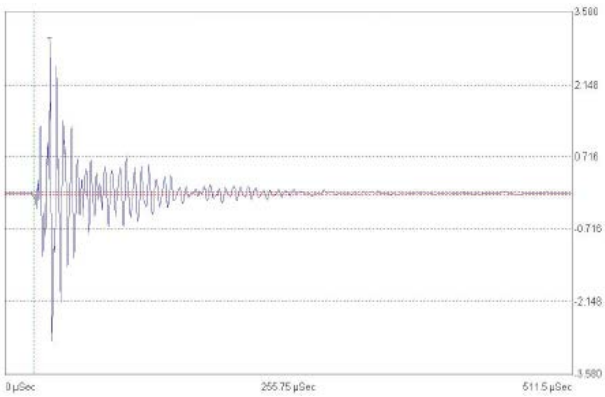

Fig.27. Wave form of fiber failure.

The bottle was ramped at a uniform pressure rate until failure and the burst pressure was recorded. A uniform pressure rate of 20bar/min was maintained for all the cycles during the pressure test. The experimental displacement of the air bottle is found to be higher than that obtained finite element analysis (figure 24). The AE data sets were generated by loading the unidirectional tensile specimens (figure 25) at a uniform rate of 5kN/min up to failure. The failure loads of each specimen were recorded.

Matrix splitting occurs when matrix cracking occurs along the fibers. This mechanism can bring down the failure load as much as the fiber failure. The duration of this failure is longer; therefore, the counts and energy are more as depicted in figure 26. The fiber breakage has a very short duration and is less in counts, as shown in figure 27. The fiber breakage is shown in figure 28 when the air bottle was tested at a pressure of 60 MPa.

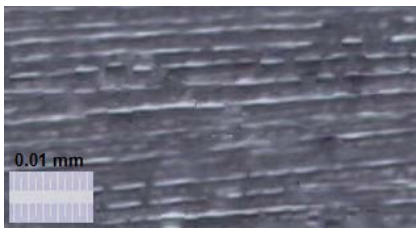

Fig.28. Wave form of fiber failure.

5 Conclusion

E-glass/epoxy composite air bottle is designed and verified using finite element analysis and experimentally to take the load of 40 MPa. The hoop and helical winding layer thicknesses are, respectively, 3.6 3.013 mm. Matrix splitting has occurred along the fibers. The fiber breakage has been observed when the air bottle was tested at a pressure of 60 MPa.

Acknowledgment

The authors wish to thank A, B, C. This work was supported in part by a grant from XYZ.

References

[1] Steven Campbell, Trans Ocean Gas Inc., "CNG transportation utilizing composite, pressure vessels," Offshore Technology Conference, 5-8 May, Houston, Texas, 2003, http://dx.doi.org/10.4043/15297-MS.

[2] William R. Gaiser, "Filament wound pressure vessel," US 5287987A.

[3] B. Kotiveerachari, A.C Reddy, "Interfacial effect on the fracture mechanism in GFRP composites," CEMILAC Conference, Ministry of Defence, India 1 (B), pp.85-87, 1999.

[4] A. Chenaakesava Reddy, "Evaluation of Curing Process for Carbon-Epoxy Composites by Mechanical Characterization for Re-entry Vehicle Structure," International Journal of Scientific & Engineering Research, vol.6, no.3, pp.65-70, 2015.

[5] A. Chennakesava Reddy, "Evaluation of Curing Process for Kevlar 49-Epoxy Composites by Mechanical Characterization Designed for Brake Liners," International Journal of Science and Research, vol.4, no.4, pp. 2365-2371, 2015.

[6] A. Chennakesava Reddy, "Evaluation of Curing Process for Bi-directional S-Glass (5HS)/Epoxy (780E +782H) Composites Fabricated by Vacuum Infusion Process for Wind Energy Blades," International Journal of Advanced Research, vol.3, no.4, pp. 667-675, 2015.

[7] AC Reddy, MV Sagar, "Two-dimensional theoretical modeling of anisotropic wear in carbon/epoxy FRP composites: comparison with experimental data," International Journal of Theoretical and Applied Mechanics, vol.6, no.1, pp.47-57, 2010.